Acta Geodyn. Geomater., Vol. 22, No. 3 (219), 413–426, 2025
DOI: 10.13168/AGG.2025.0029
journal homepage: https://www.irsm.cas.cz/acta

ORIGINAL PAPER

A DISSOLUTION MECHANICS MODEL OF LIMESTONE BASED ON HOEK-BROWN CRITERION

YanChun TANG [1, 2], QingRu WANG [1, 2], *, ZiYou XING [1, 2] and Yong XIAO [1, 2]

[1] *Key Laboratory of Geological Hazards on Three Gorges Reservoir Area, Ministry of Education, Yichang, 443002, China*
[2] *School of Civil Engineering and Architecture, China Three Gorges University, Yichang, 443002, China*

**Corresponding author's e-mail:* wang012042@163.com

ARTICLE INFO

Article history:
Received 12 May 2025
Accepted 2 September 2025
Available online 18 September 2025

Keywords:
Limestone
Dissolution
Hoek-Brown Criterion
Mechanical model
Dynamic evolution of surrounding rock stability

ABSTRACT

The dissolution-induced degradation of mechanical properties in limestone poses a significant threat to the stability of surrounding rock masses in karst environments. Combined the Geological Strength Index (GSI) with the Hoek-Brown (H-B) criterion, an integrated model is proposed to characterize the mechanical behavior of dissolving limestone. A novel parameter, the DGSI (Dissolution-affected Geological Strength Index), is established to quantify the dynamic evolution of geological strength throughout the processes of crack initiation and propagation under dissolution. Incorporated into a new C-DLMM (Crack-stage Dependent Limestone Mechanical Model), it can effectively characterize the mechanical response of limestone fracture under dissolution. Through inverse analysis of triaxial compression tests on dissolved limestone samples using a FLAC-based genetic algorithm, the time correlation between DGSI, equivalent plastic strain, and dissolution duration is revealed, verifying the scientific basis of C-DLMM. This method can evaluate the stability of limestone caverns subjected to dissolution. Numerical simulations demonstrate that under the same initial stability, the equivalent plastic strain in the surrounding rock exhibits a progressive increase over time. The zone of maximum plastic strain and 0.6 % equivalent strain profile progressively expand with continued dissolution. Compared with the non-dissolved state, the dissolution process amplifies the maximum equivalent plastic strain by 2-10 times and expands the 0.6 % strain affected zone by 4-7 times. These findings can provide a theoretical basis for understanding the stability evolution mechanism of karst cave systems and deliver practical guidance for underground engineering projects in soluble rock formations.

1. INTRODUCTION

Evaluating the impact of dissolution on the stability of limestone rock in underground caverns is critically important. A thorough understanding of the mechanical properties of dissolved limestone is essential to predict its behavior under various operational conditions. The mechanical properties of limestone subjected to dissolution have been extensively investigated globally, leading to the development of various mechanical models to characterize its behavior. In mechanical test during dissolution Laouafa et al. (2021) demonstrated that many solvable rocks will dissolve when in contact with liquids such as water, resulting in cavity formation. This process can subsequently lead to either gradual ground subsidence or collapse. Tang et al. (2021) and Wang (2019) conducted experiments on limestone samples under different initial loading and unloading conditions to examine their mechanical behavior. Their results indicated that although the mechanical failure mechanism of limestone remained unchanged during dissolution, a marked degradation in macroscopic mechanical properties was observed. The impact of dissolution on limestone rock mass changes at different stages of crack propagation. After dissolution, the limestone specimens developed additional branch cracks, which contributed to a reduction in mechanical strength by lowering the crack initiation stress and damage stress (Ding et al., 2024). The constituent minerals of carbonate rocks exhibit heterogeneous dissolution behavior. In addition, mechanical and physical weathering processes may occur around the grains. These factors indicate that the petrographic characteristics of carbonate rock play a more critical role in understanding karstification than traditional ones (Larson and Emmons, 2021). Luo et al. (2024) conducted acid- etching experiments and revealed that an increase in chemical damage would induce a transition in the fracture failure mode of limestone from single fracture to a complex multi-fracture coalescence pattern. Corvo et al. (2010) examined the degradation of large-scale chert materials used in historical buildings that affected by air pollution and water vapor in tropical humid climates. Dochez et al. (2014) explored the degradation of rainwater flint materials under similar climates through in-situ and indoor experiments. Their work addressed the chemical interaction between rainwater and chalk, as well as the mechanical responses of water-erosion-

Cite this article as: Tang YC, Wang QR, Xing ZY, Xiao Y: A dissolution mechanics model of limestone based on Hoek-Brown criterion. Acta Geodyn. Geomater., 22, No. 3 (219), 413–426, 2025. DOI: 10.13168/AGG.2025.0029

modified discontinuous surfaces. Gao et al. (2024) observed an increase in the equivalent pore size and the connectivity of rock pores post-dissolution. Gu et al. (2024) pointed out that although variations in dissolution, the stress-strain curves of greywacke still showed a consistent trend of change, and long dissolution led to a pronounced multi-peak morphology in these curves. The dissolution process involves the reaction of $CaCO_3$ with hydrogen ions in formation brine to generate soluble bicarbonate ions (HCO_3^-). This chemical process facilitates the continuous removal of carbonate material through the generation of water-soluble species, thereby driving the progressive dissolution of limestone (Al-Yaseri et al., 2023). Moras et al. (2022) showed that quicklime and slaked lime have relatively high solubilities in seawater. The dissolution of limestone is primarily driven by its reaction with hydrogen ions (H^+). Rock failure occurred when the average stress within 2L matches the tensile strength of the material (Justo et al., 2021). Seyyedi et al. (2020) verified that limestone can increase the concentration of Ca 2^+ in pore solutions, which accelerates the dissolution of C_3S and promotes the precipitation of C-A-S-H. In addition, Briendl et al. (2020) reported that vigorous dissolution of calcite led to the formation of wormholes, thereby increasing the porosity and permeability of the area and enhancing the fluid injection capacity.

In studies on the mechanical models of limestone under dissolution, Tang et al. (2021, 2008, 2023) established a deterioration model for the mechanical properties of dissolved limestone based on uniaxial compression tests. Nasr-El-Din et al. (2008) studied the impact of different acids on peak stress of rock samples. Zhang et al. (2021) divided the rock bearing capacity into elasticity and damage components, and derived a macro-micro composite damage model using the Hoek-Brown criterion. Elsworth and Yasuhara (2010) developed a simple zero-dimensional model capable of capturing complex experimental behaviors, which can serve as a constitutive model of calcite dissolution and capture key aspects of the continuous response in fracture media. Xu et al. (2021, 2020) highlighted the superiority of the H-B criterion over the Mohr-Coulomb criterion in capturing nonlinear failure behavior of rock masses, particularly in the effects of rock strength, structural planes, and stress conditions on rock mass strength. Malvoisin and Baumgartner (2021) established a quantitative model of dissolution and precipitation creep that explicitly accounts for dissolution and precipitation at the grain interface. Shi et al. (2011) established a three-dimensional damage model to explain the mechanisms of rock failure. Jin et al. (2020) introduced a rock strain softening model capable of describing the post-peak strain softening and dilatancy under different confining pressures.

Although the above studies have laid a foundation for investigating the dissolution mechanics and mechanical modeling of limestone, it ignores the dependency of dissolution effects and related stability effects of crack evolution in underground structures. To bridge these gaps, this study introduces a Dissolution-affected Geological Strength Index (DGSI) derived from an adaptation of Hoek-Brown criterion adaptation, which quantifies the dissolution impacts in the development of cracks. The C-DLMM combines crack propagation effects to comprehensively analyze the stability of underground limestone caves affected by dissolution.

2. CONSTRUCTION OF C-DLMM

In the absence of dissolution, the mechanical behavior of limestone can be effectively characterized by the Hoek–Brown strength criterion. This empirical relation integrates field geological observations with quantitative rock-mass strength through the Geological Strength Index (GSI). The GSI quantifies rock mass ranging from 0 to a soil-like condition to 100 for an intact and homogeneous material. After dissolution, the progressive degradation of limestone can be explicitly captured by introducing a dissolution-induced GSI reduction, DGSI, into the Hoek-Brown framework. Then the mechanical model C-DLMM (Crack-stage Dependent Limestone Mechanical Model) can be established to describe the mechanical behavior of limestone under dissolution.

Accordingly, this chapter will present the key components of C-DLMM from three aspects: the mechanical failure mechanism of limestone rock mass under dissolution, the theoretical foundation of C-DLMM, and its core theoretical elements (including strength criterion and flow law).

2.1. MECHANICAL FAILURE MECHANISM OF LIMESTONE ROCK MASS UNDER DISSOLUTION

As shown in Figure 1, the variation in the stability of surrounding rock in limestone underground caverns lies in the failure mechanism of the limestone rock mass during dissolution. The following observations can be made:

1. From a micromechanical perspective, as dissolution progresses, the stress intensity at the crack tip of the limestone rock mass exceeds the critical threshold, leading to crack destabilization and propagation, as shown in Figure 1(c);
2. From a macro-mechanical perspective, the mechanical strength of limestone rock mass degrades with continued dissolution. Triaxial compression tests on limestone indicate a marked reduction in the peak stress of the rock mass with dissolution as shown in Figure 1(d);
3. The analysis of the dissolution-induced failure mechanism of limestone rock mass in the different stages of crack development and propagation reveals that the progression of crack evolution and expansion, as well as the duration of dissolution, will significantly affect the stability of surrounding limestone.

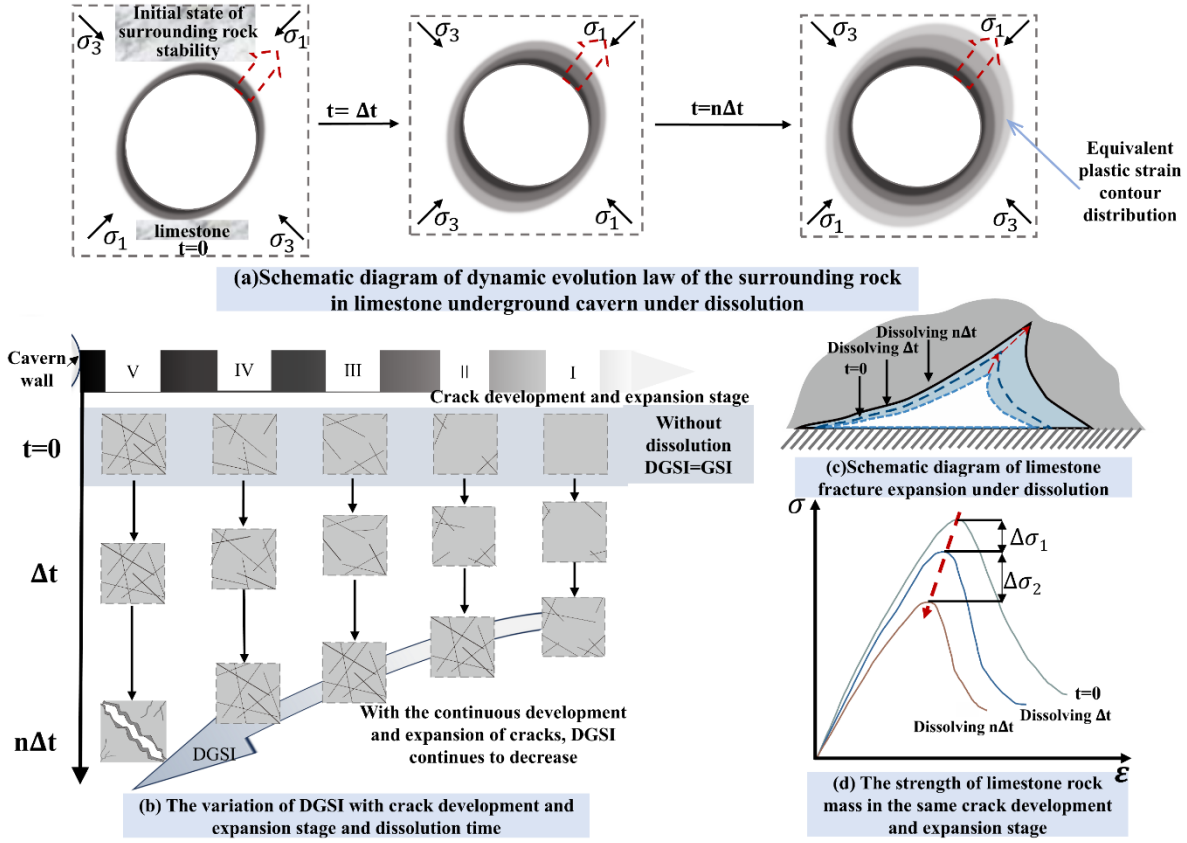

Fig. 1 Failure diagram of mechanical mechanism of limestone rock mass under dissolution.

4. Combined with the Geological Strength Index (GSI), the Hoek-Brown (H-B) criterion is used to evaluate the impact of crack propagation and expansion on the mechanical characteristics of the rock mass. In the initial stable state of limestone rock masses, the variations in crack propagation and expansion from the cavern walls to the inner rock mass may lead to different effects of dissolution on overall stability.

Therefore, within the framework of the H-B criterion, the Dissolution-affected Geological Strength Index (DGSI) can be used to evaluate the effect of dissolution in the different stages of crack propagation and expansion in limestone rock mass. This method facilitates the development of a tailored mechanical model for dissolved limestone, enabling systematic analysis of the evolving stability conditions of surrounding rock in underground limestone caverns under dissolution.

2.2. THEORETICAL BASIS AND METHODS OF C-DLMM CONSTRUCTION

The C-DLMM is established using the following methods.

2.2.1. CONSTRUCTION BASIS

1. The mechanical failure mechanism of limestone under dissolution is basically like that of limestone in an insoluble dissolution;
2. In the elastic stage of limestone sample, namely the surface meso-crack stage, dissolution has the least effect on the mechanical properties of the sample. The negligible mass difference before and after dissolution indicates that the effect of dissolution on the elastic mechanical parameters of the limestone sample can be ignored;
3. It is speculated that the tensile strength of limestone rock mass remains unchanged under dissolution.

2.2.2. CONSTRUCTION METHODS

1. Based on the H-B criterion, DGSI is introduced to quantify the effect of dissolution on the different stages of crack development and expansion in limestone rock masses;
2. The impact of dissolution on the mechanical properties of intact limestone blocks can be ignored (Moras et al., 2022). In this way, it is reasonable to assume that the uniaxial compressive strength (σ_{c_i}) of intact rocks remains constantunder dissolution.

2.3. THEORETICAL RELATION OF C-DLMM

2.3.1. STRENGTH CRITERION

The strength criterion of C-DLMM is expressed as follows (He and Tang, 2024):

$$\sigma_1 = \sigma_3 + \sigma_{\mathrm{ci}} \left(m_b^* \frac{\sigma_3}{\sigma_{ci}} + s^* \right)^{a^*} \quad (1)$$

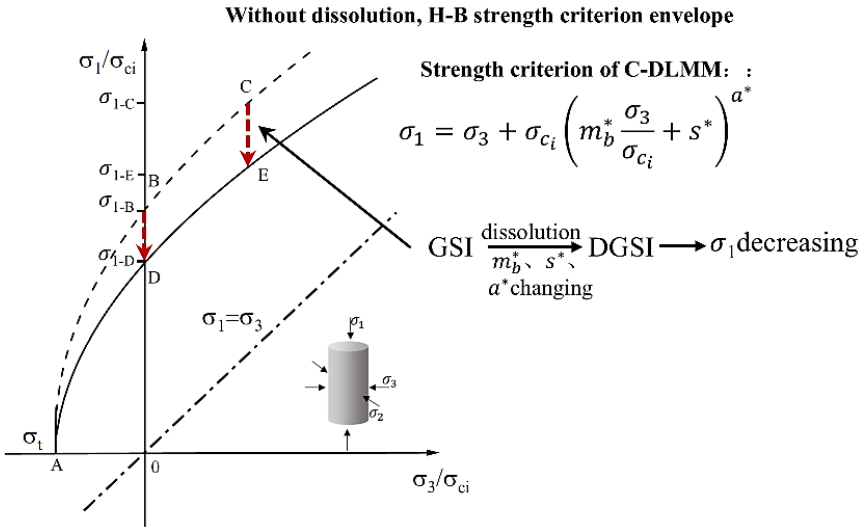

Fig. 2 Diagram of C-DLMM strength criterion.

where σ_{c_i} represents the uniaxial compressive strength of the rock sample; the empirical parameters m_b^*, $s^*$and a^*present the characteristics of rock mass and are all correlated with the DGSI.

m_b^*,$s^*$and $a^*$are expressed as follows (He and Tang, 2024):

$$\begin{cases} m_b^* = m_i \, exp\left(\frac{DGSI-100}{28-14D}\right) \\ s^* = exp\left(\frac{DGSI-100}{9-3D}\right) \\ a^* = \frac{1}{2} + \frac{1}{6}\left(exp\left(\frac{-DGSI}{15}\right) - exp\left(\frac{-20}{3}\right)\right) \end{cases} \quad (2)$$

where, m_i represents the limestone in the range of 12± 3; D represents the disturbance factor of rock mass. In the absence of dissolution, m_b^*, s^* and $a^*$are equal to m_b, s and a in the H-B criterion (Hoek and Diederichs, 2006).

The schematic diagram of C-DLMM strength criterion is shown in Figure 2:

1. The solid line ADE reflects the envelope of the C-DLMM strength criterion, as calculated in Eq. (1). It can be seen from Eq. (2) that m_b^*,s^* and a^* are controlled by DGSI. Therefore, the alteration of ADE is influenced by DGSI;
2. The dotted line ABC represents the H-B strength criterion envelope without dissolution. The shapes of ADE and ABC are similar. The difference is that at the dissolution time t=0, DGSI equals GSI. As the dissolution time increases, GSI diminishes to DGSI, and the H-B strength criterion envelope begins to transition to the C-DLMM strength criterion envelope;
3. Under the same σ_3, points C to E indicate that as the DGSI changes, the peak stress of limestone rock mass shifts fromσ_{1-C} to σ_{1-E}. When σ_3 = 0, points B to D reflect the progression of peak stress of limestone rock mass changing with DGSI under uniaxial compression.

2.3.2. FLOW RULE

The flow law of C-DLMM is elucidated by Eq. (3), which describes the relationship between the normal direction of the yield surface and the plastic increment caused by dissolution (due to stress changes).

$$\Delta e_1^p = \gamma^* \Delta e_3^p \quad (3)$$

where, the flow coefficientγ* is related to the stress and degree of dissolution, γ* is affected by the change of DGSI. When the dissolution time is 0, the flow coefficient γ* is equal to the flow coefficient γ without dissolution. The flow law under different confining pressures is shown in Eq. (4).

$$\begin{cases} \gamma_{rf}^* = \gamma_{rf} = \frac{\sigma_1}{\sigma_3}\left(\sigma_3 < 0\right) \\ \gamma_{af}^* = -\frac{1}{1+\frac{1}{2}\sigma_{ci}\left(m_b^*\sigma_3/\sigma_{ci}+s^*\right)^{-\frac{1}{2}}\left(m_b^*/\sigma_{ci}\right)}\left(\sigma_3 = 0\right) \\ \gamma_{cv}^* = \gamma_{cv} = 1\left(\sigma_3 > \sigma_{cv}\right) \\ \gamma_{cf}^* = \frac{1}{1/\gamma_{af}^* + \left(1/\gamma_{cv}^* - 1/\gamma_{af}^*\right)\sigma_3/\sigma_1}\left(0 < \sigma_3 \le \sigma_{cv}\right) \end{cases} \quad (4)$$

The flow coefficient γ^* is related to the magnitude of stressunder dissolution, and its variation with stress is shown in Figure 3.

1. When σ_3< 0, the flow coefficient is γ^*=γ_{rf}^*=γ_{rf} under dissolution. That is, under uniaxial compression (when σ_3< 0), the flow coefficients with and without dissolution are identical and equal to the ratio of σ_1 to σ_3;

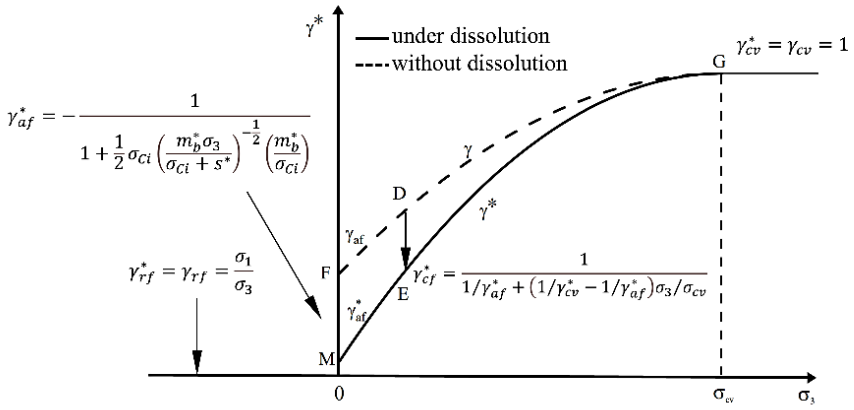

Fig. 3 Schematic diagram of flow coefficient γ*changing with confining pressure under dissolution.

2. When σ_3=0, the flow coefficient is $\gamma^*=\gamma^*_{af}$ under dissolution. From Eq. (4), γ^*_{af} is a function related to m_b^*, $s^*$and a^*. Under dissolution, γ^*_{af} is smaller than the flow coefficient γ_{af} without dissolution.
3. When $\sigma_3 > \sigma_{cv}$, the flow coefficient is $\gamma^*=\gamma^*_{cv}=\gamma_{cv}$=1under dissolution, that is, when the confining pressure reaches the anti-expansion confining pressure, the flow coefficients without dissolution and under dissolution are equal to 1;
4. When $0 < \sigma_3 \leq \sigma_{cv}$, the flow coefficient $\gamma^*=\gamma^*_{cf}$ under dissolution. From Eq. (4), $\gamma^*_{cf}$is a function related toγ^*_{af}, γ^*_{cv}, $\sigma_3$and σ_{cv}. Points D and E are the flow coefficients of limestone before and after dissolution under the same confining pressure, which means dissolution will lead to a decrease in the flow coefficient of limestone.

3. PARAMETER ACQUISITION AND RATIONALITY VERIFICATION OF C-DLMM

Based on the Hoek Brown standard and triaxial compression mechanical test data of limestone under dissolution, the DGSI values corresponding to different stages of crack propagation and expansion at different dissolution times are determined using a FLAC-based genetic algorithm. The validity is subsequently verified through comparison between experiments and numerical simulation.

3.1. USING FLAC-GENETIC ALGORITHM TO SOLVE THE PARAMETERS OF C-DLMM

The influence of the same dissolution time on the mechanical properties of limestone changes significantly in the different stages of crack development and expansion. To validate the accuracy of this point, a triaxial compression test was conducted on limestone specimens under dissolution. The experimental procedure involved an initial loading phase, followed by unloading at different stages of crack development and expansion (referred to as unloading points). The unloaded limestone samples were then placed in a solution with a pH of 3.5 (a value higher than that of natural environment from which the samples were sourced to reduce the dissolution time required for the test) for different dissolution times. The limestone samples used in this experiment were obtained from the Huanghua limestone mining area in Yichang, Hubei Province. The limestone sample is bluish-gray. The main mineral components of the rock are calcite and dolomite. Under the action of local weakly acidic groundwater, $CaCO_3$ in the calcite may react with H^+ in groundwater, leading to the dissolution of limestone. Although dolomite is also susceptible to dissolution, the process occurs at a significantly slower rate. The dissolution of the trace mineral pyrite will produce strong acid, further accelerating the overall dissolution process. The limestone sample is a cylinder with a diameter of 50mm and a height of 100 mm. Mechanical loading was carried out on a self-balancing rock true three-axis compressor (SRT). Subsequently, the limestone samples under dissolution were reloaded until failure. The mechanical failure modes of limestone under different stages of crack development and expansion, as well as different dissolution times were determined, as shown in Table 1. Based on C-DLMM, FLAC genetic algorithm is used to invert DGSI. The specific process is as follows:

1. FLAC3D computational software and the Hoek-Brown (H-B) model are used to numerically simulate the testing process. Assuming m_b=m_i, s=1, a=0.5, the parameters σ_{ci} and m_i are determined through least squares fitting;
2. Based on the above experimental data, the stress peaks corresponding to different unloading points and dissolution times are determined, and a nonlinear evolution model equation for DGSI under dissolution is formulated. The DGSI fitting is calculated as follows:

$$DGSI = f(t, \varepsilon^p)GSI \quad (5)$$

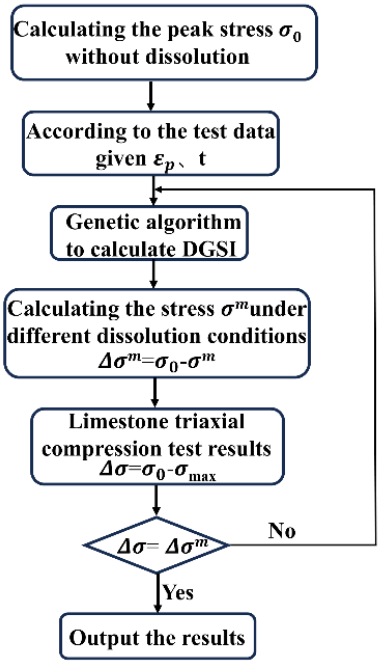

Fig. 4 Flow chart of solving DGSI based on the FLAC-genetic algorithm.

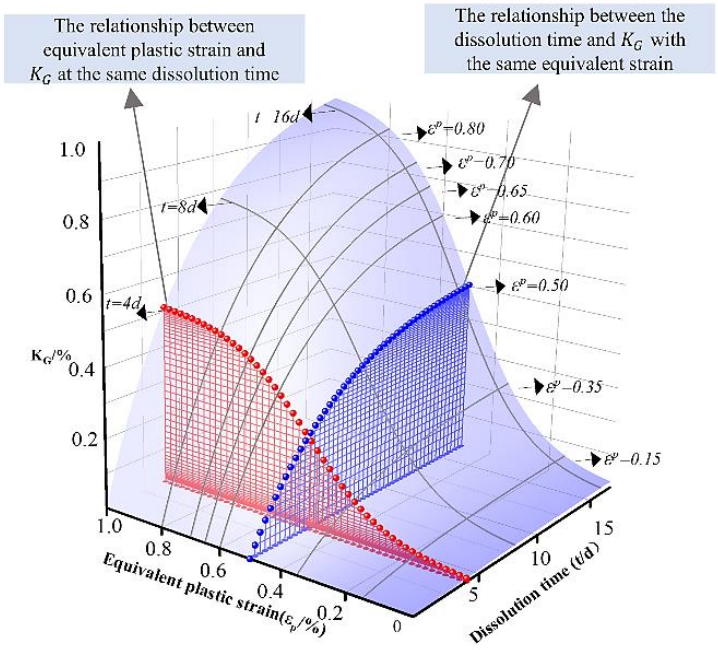

Fig. 5 The relationship between K_G and dissolution time and equivalent plastic strain.

where t represents the dissolution time, and ε^p represents the equivalent plastic strain;

3. The genetic algorithm is used to search the DGSI value after dissolution and generate a series of DGSI values;
4. According to change the calculation parameter DGSI, the DGSI value obtained by the genetic algorithm is input into the FLAC calculation model and the stress peak σ^{m*} at that moment is calculated using C-DLMM;
5. Comparing σ^{m*} with the experimental value σ^m, when $\sigma^{m*}=\sigma^m$, the DGSI values under different ε^p and t can be obtained. If these two values are not equal, the genetic evolution of the stress peak σ^{m*} after dissolution continues, and the third, fourth and fifth steps are calculated again.

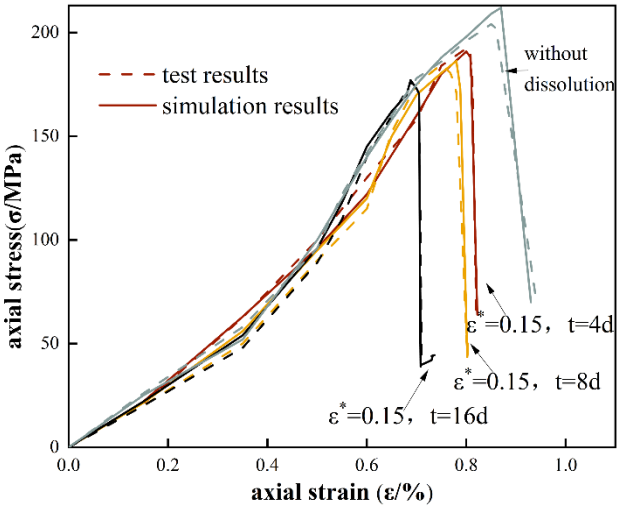

Fig. 6 Comparison of fitting and experimental results.

3.2. ANALYSIS OF THE VARIATION OF DGSI UNDER DISSOLUTION

To more intuitively analyze the variation law of geological strength index under different crack development and expansion stages under dissolution, a quantitative equation is defined to describe the change of geological strength index DGSI. The equation is defined as follows:

$$K_G = \frac{GSI - DGSI}{GSI} \tag{6}$$

where K_G is the percentage of the reduction of geological strength index under dissolution.

The DGSI value under dissolution is obtained using the FLAC-genetic algorithm. Then K_G, the percentage of geological strength index reduction under dissolution, is obtained by Eq. (6). The least squares method is then applied to fit the data. The relationship between K_G and dissolution time with the equivalent plastic strain is calculated as follows:

$$K_G = 15\left(1 - \frac{1}{1+e^{8(\varepsilon^p - 0.5)}}\right)\left(1 - e^{-t/6}\right) \tag{7}$$

The relationship between K_G and dissolution time t and the equivalent plastic strain ε^p is shown in Figure 5.

3.3. RATIONALITY VERIFICATION OF C-DLMM

A comparison between the test and simulation results of triaxial compression mechanical for limestone under dissolution is shown in Table 1. Figure 6 shows the comparison of stress-strain curves of the tests and numerical simulation under different dissolution.

1. The triaxial compression mechanical test results of limestone under dissolution are different from the calculated data in peak stress and residual stress values, although the trend in the failure stage is basically consistent. There is a close correspondence between the test results and simulation results before reaching the peak stress;
2. The difference between experimental and calculated results is usually within 2%. The above analysis indicates that the C-DLMM model can accurately capture the mechanical properties of limestone under dissolution.

4. NUMERICAL ANALYSIS OF DYNAMIC EVOLUTION LAW OF THE STABILITY OF SURROUNDING ROCK IN LIMESTONE UNDERGROUND CAVERN UNDER DISSOLUTION

Based on the C-DLMM, a stability assessment methodology for surrounding rock in limestone underground caverns under dissolution conditions is established. Furthermore, the temporal evolution behavior of the surrounding rock under such conditions is systematically analyzed.

4.1. CALCULATION METHOD FOR THE STABILITY OF SURROUNDING ROCK UNDER DISSOLUTION

The stability assessment methodology for the surrounding rock mass in limestone underground caverns during dissolution is shown in Figure 7, detailed as follows:

1. An underground cavern model is established, and the initial stability of the surrounding rock (graded by rock mass quality) is defined. Combined the FLAC^{3D} computational software with the H-B failure criterion, the pre-dissolution stability of the surrounding rock in limestone underground caverns is calculated. At the initial time point t=0, the initial stress field $\sigma_{t=0}$ and the distribution of equivalent plastic strain $\varepsilon^p_{t=0}$ within the stable surrounding rock are determined;

Table 1 Comparison of experimental data and simulation data of limestone triaxial compression mechanics under dissolution.

t/d	ε^p/%	σ_m/MPa		σ^*_m/MPa	Discrepancy/%	t/d	ε^p/%	σ_m/MPa		σ^*_m/MPa	Discrepancy/%	t/d	ε^p/%	σ_m/MPa		σ^*_m/MPa	Discrepancy/%
		Test result	Average	Simulation test				Test result	Average	Simulation test				Test result	Average	Simulation test	
		208.9															
0	0	206.7	208.2	207.7	0.24	----------											
		209.1															
		192.8						185.1						180.4			
	0.15	189.3	192.3	190.8	0.78		0.15	180.4	186.3	182.6	1.99		0.15	178.1	180.3	179.2	0.61
		194.7						193.5						182.5			
		188.1						170.3						175.4			
	0.35	180.4	182.5	181.6	0.49		0.35	180.7	174.8	174.3	0.29		0.35	169.6	171.4	168.2	1.86
		178.9						173.4						169.3			
		165.3						163.3						150.7			
	0.5	170.4	171.3	172.6	0.76		0.5	162.7	162.2	161.2	0.62		0.5	148.1	148.3	149.5	0.81
		178.2						160.6						146.2			
		167.9						150.4						135.4			
4	0.6	162.4	163.5	165.4	1.16	8	0.6	149.3	146.8	152.2	3.67	16	0.6	141.6	138.1	141.2	2.24
		160.3						140.8						137.4			
		158.4						140.1						128 .1			
	0.65	150.6	152.8	155.3	1.63		0.65	137.6	137.0	138.3	0.95		0.65	132.7	124.1	123.2	0.73
		149.5						133.4						126.6			
		138.1						122.2						120.4			
	0.7	140.7	140.1	138.9	0.86		0.7	125.4	122.5	123.2	0.57		0.7	121.9	120.2	117.9	1.91
		141.6						120.0						118.3			
		136.8						110.2						100.6			
	0.8	130.7	135.2	133.7	1.11		0.8	113.7	114.3	116.2	1.66		0.8	108.4	102.6	103..0	0.38
		137.6						119.1						98.9			

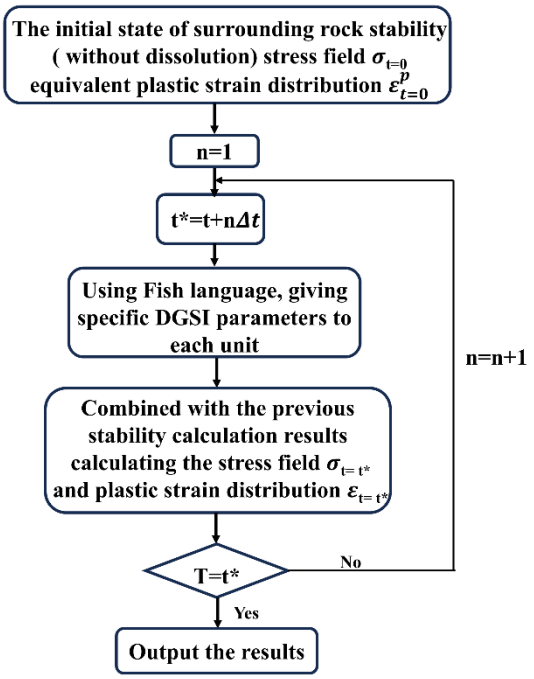

Fig. 7 Calculation method for the stability of surrounding rock in limestone underground cavern under dissolution.

2. After temporal discretization with a time increment Δ t, the Fish language scripting is used to assign the Discrete Element Grid Stabilization Index (DGSI) to each numerical grid, in conjunction with the constitutive relation given by with Eq. (7);
3. At the beginning of dissolution (t=0), the stability of the surrounding rock at time t =Δt is simulated numerically, leveraging the initial stress field $\sigma_{t=}\Delta t$ and the equivalent plastic strain distribution $\varepsilon^p_{t=\Delta t}$. Therefore, the stress field at time t =Δt is derived, denoted as $\sigma_{t=}\Delta t$, and the corresponding equivalent plastic strain distribution $\varepsilon^p_{t=\Delta t}$ is derived;
4. As the dissolution time increases, the stability of the surrounding rock will be updated based on previous simulation results. The DGSI for each grid is recalculated using Fish language, and the stress field $\sigma_{t=n\Delta t}$ and equivalent plastic strain distribution $\varepsilon^p_{t=n\Delta t}$ are determined at each time step.
5. The computation proceeds iteratively through step 4, with the dissolution time t* incrementally increased until it equals the total dissolution time T. After reaching this criterion, the final stress field and equivalent plastic strain distribution are obtained. If t* is smaller than T, the process returns to step 4 and repeats until the total dissolution time T is achieved, thereby generating the stress field and equivalent plastic strain distribution at time t.

4.2. ANALYSIS OF DYNAMIC EVOLUTION LAW OF SURROUNDING ROCK STABILITY OF UNDERGROUND CAVERN LIMESTONE UNDER DISSOLUTION

A circular cavern model with a diameter of 10 meters is constructed using the established stability calculation method for the surrounding rock of limestone underground caverns under dissolution. The parameters are set as D=0, m_i=9 (Liu et al., 2013; Sun et al., 2004), with a Poisson ratio of 0.22 and a density of 2750 kg/m^3. The dynamic evolution of the stability of surrounding rock in limestone caves is studied from two key aspects: the plastic behavior and displacement characteristics of the surrounding rock. This analysis is based on different initial states of rock stability.

4.2.1. ANALYSIS ON THE EVOLUTION LAW OF PLASTIC CHARACTERISTICS OF LIMESTONE SURROUNDING ROCK IN UNDERGROUND CAVERN UNDER DISSOLUTION

The evolution of plastic behavior in the limestone surrounding rock of an underground cavern during dissolution is shown in Figure 8. It shows the evolution of the maximum equivalent plastic strain of limestone surrounding rock, the volume of the plastic zone, the area of surrounding rock corresponding to an equivalent plastic strain of 0.6 %, and the equivalent plastic strain at each monitoring point at different dissolution times under three different initial stable states of surrounding rock. As shown in Figure 8, as the initial stability of the limestone surrounding rock deteriorates, the higher the overall level of the curve represented by the above parameters and the faster the growth rate. This indicates that the surrounding rock enters the plastic state earlier and continues to expand.

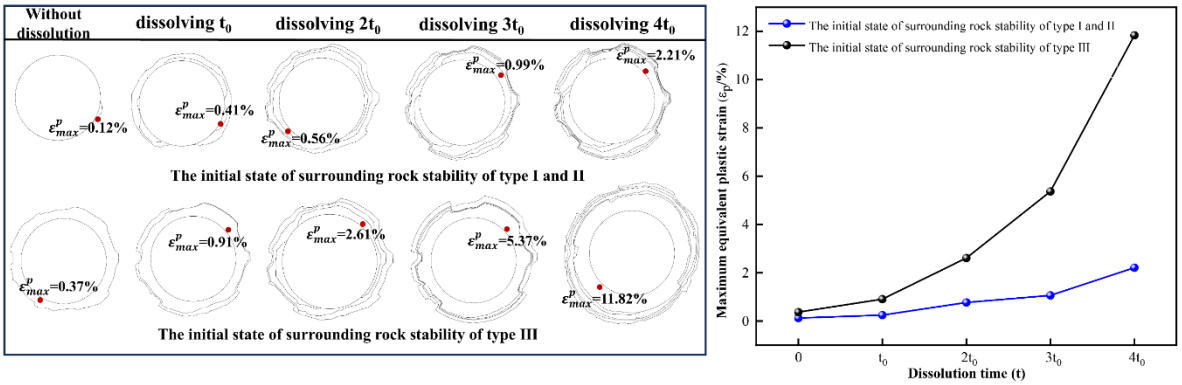

(a)The evolution law of maximum equivalent plastic strain of limestone in the different initial states of surrounding rock stability

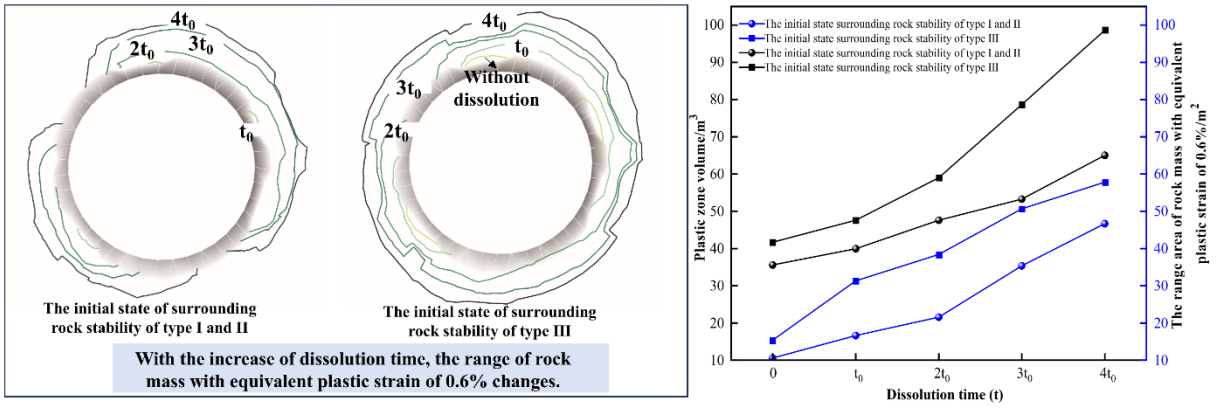

(b)The evolution law of plastic zone volume and equivalent plastic strain corresponding to 0.6 % under different initial states of surrounding rock stability

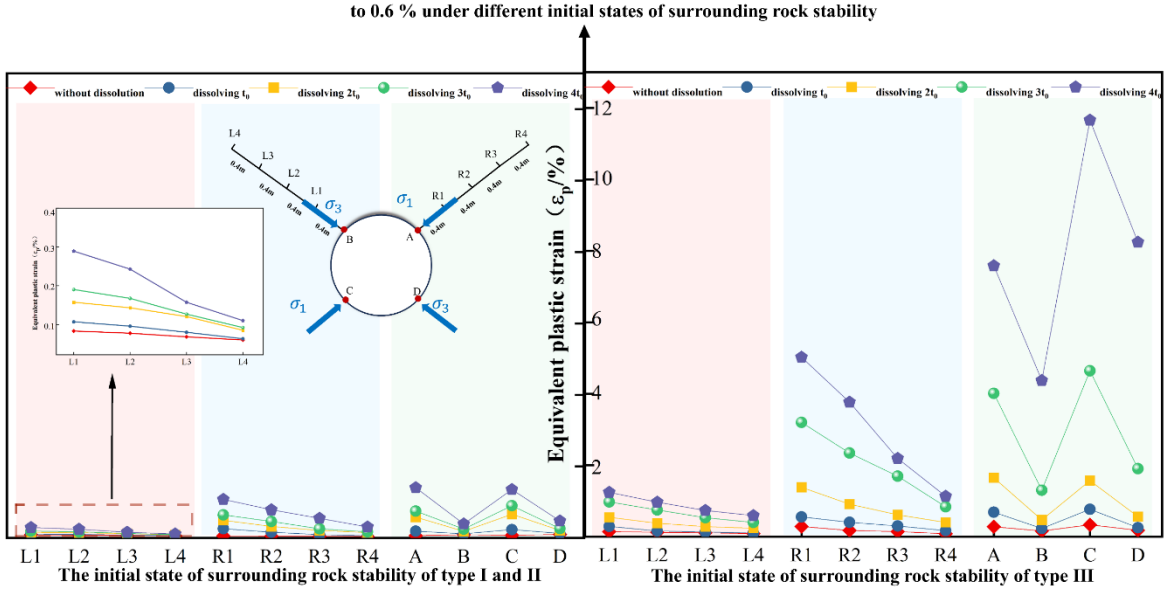

(c)The evolution law of equivalent plastic strain of each monitoring point in different initial states of surrounding rock stability

Fig. 8 Evolution law of plastic characteristics of surrounding rock in limestone underground cavern under dissolution.

The stability of the surrounding rock in limestone underground caverns under different initial states is subject to dissolution-induced alterations. The following observations are derived from the analysis:

1. As shown in Figure 8(a), at the same initial stable state, the equivalent plastic strain in the surrounding limestone rock increases with continued dissolution. For the initial stability state of type I and II surrounding rocks, after complete dissolution (4 t_0), the peak equivalent plastic strain is 2.2 %, with an increase of 2.1 % compared to the maximum strain in the undissolved state. In contrast, for the initial stability state of type III surrounding rock, the strain increases to 11.8 % at 4 t_0, with an increase of 11.4 % compared to the undissolved state;

2. Figure 8(b) shows that, under stable initial conditions, the volume of the plastic zone and the area exhibiting an equivalent plastic strain of 0.6 % expands with progressive dissolution. In the initial stability state of type I and II surrounding rock, the area with an equivalent plastic strain of 0.6 % reaches about 46.7 m² at 4 t_0, which is 4.4 times higher than the undissolved state. At the same time, the volume of plastic zone expands to 65.1 m³, which is 1.8 times the dissolution time. For the initial stability state of type III surrounding rock, the area with an equivalent plastic strain of 0.6 % at 4 t_0 is 57.8 m², which is 3.8 times larger than that without dissolution. The volume of the plastic zone increases to 98.6 m³, which is 2.4 times that of the undissolved state;
3. Figure 8(c) shows that under dissolution, the equivalent plastic strain in the surrounding rock of limestone caverns decreases with the distance from the cavern wall. Due to the direction of the maximum principal stress, the monitoring point on the right always has a higher strain than that on the left. As the dissolution proceeds, the strain at monitoring points A and C becomes increasingly different from that at points B and D, reflecting the influence of the direction of the maximum principal stress. When there is no dissolution, the strain values at all monitoring points are relatively uniform; as dissolution proceeds, differences appear and expands, especially between points A/C and B/D.

4.2.2. ANALYSIS OF DISPLACEMENT EVOLUTION LAW OF LIMESTONE SURROUNDING ROCK IN UNDERGROUND CAVERNS UNDER DISSOLUTION

Figure 9 shows the displacement progression of limestone surrounding rock in underground caverns throughout the entire dissolution. It shows the evolution of the maximum displacement of limestone surrounding rock, the displacement 0.006 m contour line of the surrounding rock area, and the displacement at each monitoring point with different dissolution times under three different initial stable states of surrounding rock.

As shown in Figure 9, as the initial stability of the limestone surrounding rock decreases, the displacement and the growth rate increased markedly. This trend indicates that the instability of the surrounding rock occurs earlier and the deformation is more significant.

Figure 9 shows the displacement of the surrounding rock in limestone underground caverns under different initial states during dissolution. Specific trends are drawn as follows:

1. As shown in Figure 9(a), for caverns with the same initial stability, the displacement of limestone surrounding rock increases gradually with continued dissolution. When the limestone is in the initial stability state of type I and II surrounding rock, the maximum displacement reaches 0.018 meters at 4 t_0, exceeding the undissolved state by 0.012 meters. For limestone in the initial stability state of type III surrounding rock, the maximum displacement at 4 t_0 is 0.054 meters, with an increase of 0.046 meters compared to the undissolved state;
2. Figure 9(b) shows that at the same initial stability, the displacement in the limestone surrounding rock broadens 0.006 meters over the dissolution time. For the initial stability of type I and II surrounding rock, the area affected by a displacement of 0.006 meters is 70.1m² at 4 t_0, which is 4.2 times the area without dissolution. For the initial stability of type III, this area is 88.5 m², which is 4.0 times larger than the undissolved state;
3. Figure 9(c) shows that the impact of dissolution on the displacement of the surrounding rock decreases as the distance from cavern walls increases. The displacement of each monitoring point increases as the dissolution time increases. Initially, without dissolution, the displacement of monitoring points is consistent. However, under dissolution, the displacement difference between points A /C and points B/D increases under the influence of the direction of the maximum principal stress. Starting from the dissolution of 2 t_0, significant displacement is observed at all four monitoring points, and the differences between them gradually decreased over time.

5. CONCLUSIONS

Based on the H-B criterion, a Dynamic Geological Strength Index (DGSI) is proposed, and a C-DLMM model is developed to characterize the mechanical behavior of limestone at different degrees of fracture development and propagation under dissolution. This model can effectively quantify the strength degradation induced by dissolution at different stages of fracture development and propagation. The proposed framework further enables an enhanced stability assessment of surrounding rock in limestone underground caverns under dissolution conditions.

The main contributions of this study are summarized as follows:

1. A model (C-DLMM) was established to characterize the mechanical properties of limestone affected by different stages of fracture development and propagation under dissolution. The evolution of DGSI with dissolution time and equivalent plastic strain was determined, and a stability calculation method for underground limestone surrounding rock under dissolution was constructed;
2. The stability evaluation method for limestone surrounding rock in underground caverns under dissolution was implemented numerically using FLAC3D software. The dynamic evolution of the stability of limestone surrounding rock in

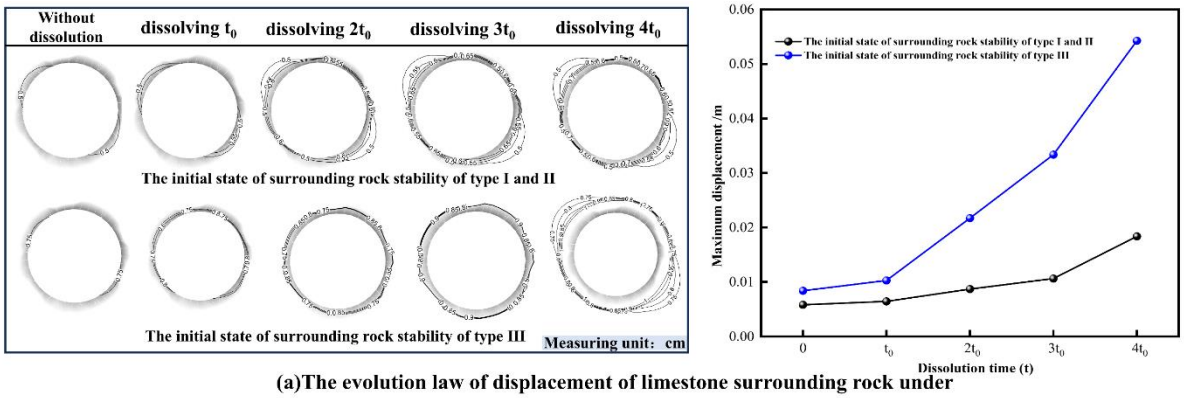

(a)The evolution law of displacement of limestone surrounding rock under different initial states of surrounding rock stability

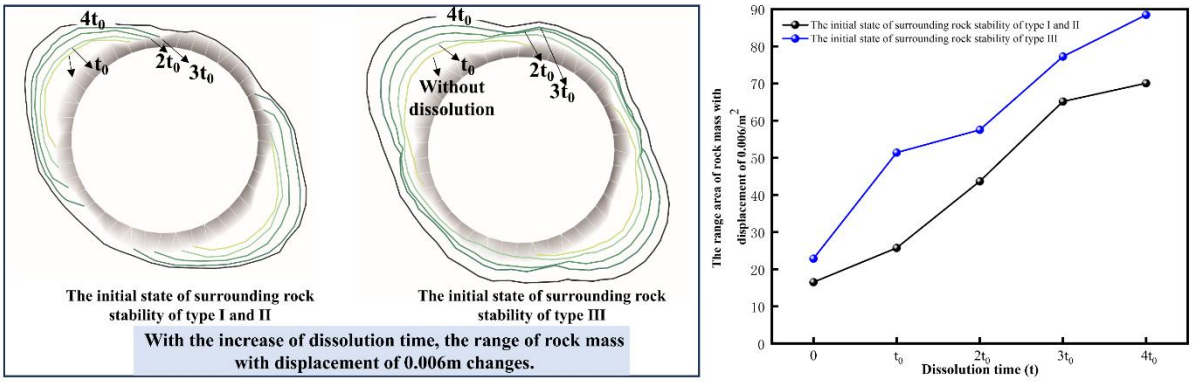

(b)The evolution law of displacement corresponding to 0.006m under different initial states of surrounding rock stability

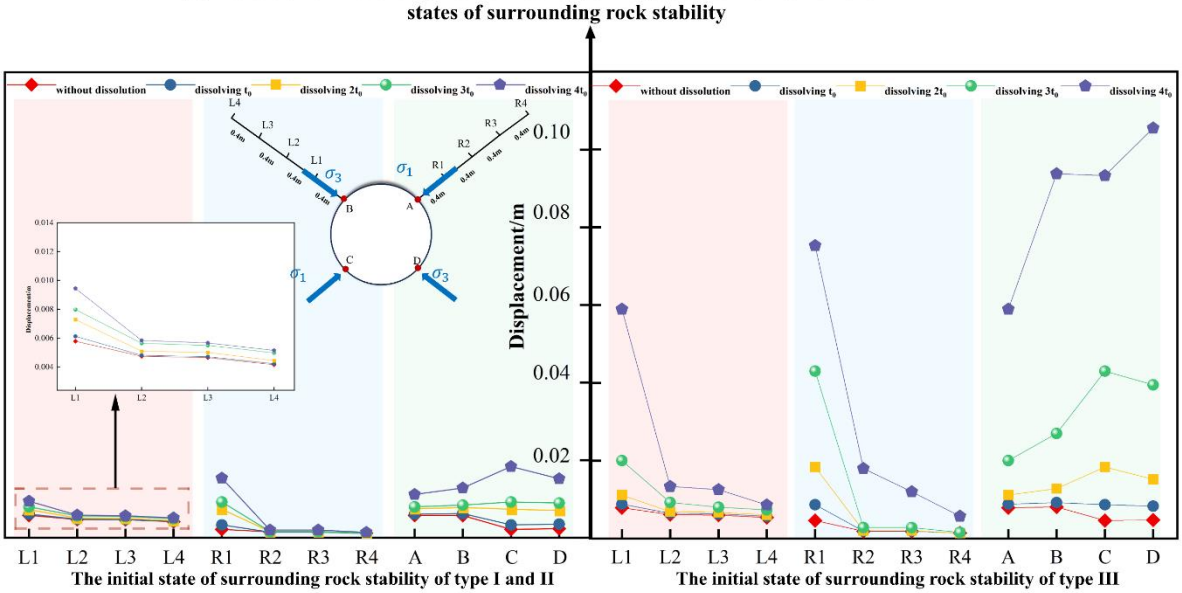

(c)The evolution law of displacement of each monitoring point in different surrounding rock stability states

Fig. 9 Displacement evolution of surrounding rock in limestone underground cavern under dissolution.

underground caverns is analyzed from two aspects: the plastic characteristics of the surrounding rock and the displacement. The results show that the worse the initial stability state of the surrounding rock is (such as Class III surrounding rock), the more significant the increases in plastic strain and displacement caused by dissolution, and the faster the stability degradation. The C-DLMM model provides a dynamic analysis for the long-term stability assessment of limestone surrounding rock in dissolution-fracture coupled environments. It can support on-site risk early warning, prevention, and control of underground engineering in karst areas to a certain extent.

REFERENCES

Al-Yaseri, A., Al-Mukainah, H. and Yekeen, N.: 2023, Experimental insights into limestone-hydrogen interactions and the resultant effects on underground hydrogen storage. Fuel, 344, 128000. DOI: 10.1016/j.fuel.2023.128000

Briendl, L.G., Mittermayr, F., Baldermann, A., Steindl, F.R., Sakoparnig, M., Letofsky-Papst, I. and Galan, I.: 2020, Early hydration of cementitious systems accelerated by aluminiumsulphate: Effect of fine limestone. Cem. Concr. Res., 134, 106069. DOI: 10.1016/j.cemconres.2020.106069

Corvo, F., Reyes, J., Valdes, C., Villaseñor, F., Cuesta, O., Aguilar, D. and Quintana, P.: 2010, Influence of air pollution and humidity on limestone materials degradation in historical buildings located in cities under tropical coastal climates. Water Air Soil Pollut., 205, 359–375. DOI: 10.1007/s11270-009-0081-1

Ding, C., Zuo, S., and Mo, Y.: 2024, Study on the mechanical and damage properties of laminated limestone under acid mine drainage dissolution. Geomech. Geophys. Geo-Energy Geo-Resour., 10, 97. DOI: 10.1007/s40948-024-00820-7

Dochez, S., Laouafa, F., Franck, C., Guedon, S., Martineau, F., d'Amato, J. and Saintenoy, A.: 2014, Multi-scale analysis of water alteration on the rockslope stability framework. Acta Geophys., 62, 5, 1025–1048. DOI: 10.2478/s11600-014-0232-7

Elsworth, D. and Yasuhara, H.: 2010, Mechanical and transport constitutive models for fractures subject to dissolution and precipitation. Int. J. Numer. Anal. Methods Geomech., 34, 5, 533–549. DOI: 10.1002/nag.831

Gao, P., Qi, X., Xie, Y.L., Wang, X.H. and Wang, Y.H.: 2024, Study on microstructure and change rule of calcite bearing vein limestone dissolution based on CT imaging technology. J. Eng. Geol., 1–14. DOI: 10.13544/j.cnki.jeg.2024-0318

Gu, J.H., Guo, J.Q., Wang, E.B., Chen, F. and Li, S.H.: 2024, Mechanical properties and energy evolution characteristics of Brazilian splitting of limestone with different dissolution degrees. Mining Research and Development, 44, 10, 115–124, (in Chinese). DOI: 10.13827/j.cnki.kyyk.2024.10.014

He, C.H. and Tang, Y.C.: 2024, Calculation method of mechanical parameters of limestone under dissolution based on Hoek-Brown strength criterion. Journal of China Three Gorges University (Natural Sciences), 46, 5, 62–67. DOI: 10.13393/j.cnki.issn.1672-948X.2024.05.010

Hoek, E. and Diederichs, M.S.: 2006, Empirical estimation of rock mass modulus. Int. J. Rock Mech. Min. Sci., 43, 2, 203–215. DOI: 10.1016/j.ijrmms.2005.06.005

Jin, J.C., She, C.X. and Shang, P.Y.: 2020, A strain-softening model of rock based on Hoek-Brown criterion. Rock Soil Mech., 41, 3, 939–951. DOI: 10.16285/j.rsm.2019.0539

Justo, J., Castro, J., and Cicero, S.: 2021, Application of the Theory of Critical Distances for the fracture assessment of a notched limestone subjected to different temperatures and mixed mode with predominant mode I loading conditions. Rock Mech. Rock Eng., 54, 5, 2335–2354. DOI: 10.1007/s00603-021-02365-7

Laouafa, F., Guo, J. and Quintard, M.: 2021, Underground rock dissolution and geomechanical issues. Rock Mech. Rock Eng., 54, 7, 3423–3445. DOI: 10.1007/s00603-020-02320-y

Larson, E.B., and Emmons, R.V.: 2021, Dissolution of carbonate rocks in a laboratory setting: rates and textures. Minerals, 11, 6, 605. DOI: 10.3390/min11060605

Liu, N., Zhang, C.S., Chu, W.J. and Wu, X.M.: 2013, Excavation damaged zone characteristics in deep tunnel of JinPing II hydropower station. Chin. J. Rock Mech. Eng., 32, 11, 2235–2241.

Luo, Z.S., Zhao, L.Y., Cao, X., Zhang, X. and Deng, H.F.: 2025, Study on tensile properties and chemical damage mechanism of limestone under acid etching. J. Eng. Geol., 33, 4, 1343 – 1353. DOI: 10.13544/j.cnki.jeg.2023-0209

Malvoisin, B. and Baumgartner, L.P.: 2021, Mineral dissolution and precipitation under stress: model formulation and application to metamorphic reactions. Geochem. Geophys. Geosyst., 22, 5, e2021GC009633. DOI: 10.1029/2021GC009633

Moras, C.A., Bach, L.T., Cyronak, T., Joannes-Boyau, R. and Schulz, K.G.: 2022, Ocean alkalinity enhancement–avoiding runaway $CaCO_3$ precipitation during quick and hydrated lime dissolution. Biogeosciences, 19, 15, 3537–3557. DOI: 10.5194/bg-19-3537-2022

Nasr-El-Din, H.A., Al-Driweesh, S.M., Metcalf, A.S. and Chesson, J.B.: 2008, Fracture acidizing: What role does formation softening play in production response? SPE Prod. Oper., 23, 2, 184–191. DOI: 10.2118/103344-PA

Seyyedi, M., Mahmud, H.K.B., Verrall, M., Giwelli, A., Esteban, L., Ghasemiziarani, M. and Clennell, B.: 2020, Pore structure changes occur during CO_2 injection into carbonate reservoirs. Sci. Rep., 10, 1, 3624. DOI: 10.1038/s41598-020-60247-4

Shi, C., Jiang, X.X., Zhu, Z.D. and Hao, Z.Q.: 2011, Study on rock damage constitutive model based on Hoek Brown criterion and its parameters. Chin. J. Rock Mech. Eng., 30, S1, 2647-2652.

Sun, H.Y., Shang, Y.Q. and Zhang, C.S.: 2004, Numerical modeling analysis for surrounding rockmass stability of large underground cavities. J. Zhejiang Univ. Sci. (Engineering Science), 1, 71-74+86

Tang, Y.C., Li, B.H., Zhu, Z.M., Zhen, Y.Z., Zhang, C.Q. and Zhou, H.: 2021, Experimental study on influence from karstification on mechanical properties of parallel and vertical bedding-planes of layered limestone. Water Resources and Hydropower Engineering, 52, 8, 149–161. DOI: 10.13928/j.cnki.wrahe.2021.08.015

Tang, Y.C., Liu, Y., He, C.H., Shang, Y.F.: 2023, Deterioration model of mechanical properties of limestone considering dissolution. Chin. J. Rock Mech. Eng., 42, S2, 4091–4098. DOI: 10.13722/j.cnki.jrme.2022.1110

Tang, Y.C., Zhou, H., Feng, X.T. and Xie, Y.T.: 2008, Study on dissolving model under effect of stress for rock salt. Rock Soil Mech., 2, 296–302. DOI: 10.16285/j.rsm.2008.02.049

Tang, Y.C. and Zhou, H.: 2012, Study of plastic mechanical model of rock salt with dissolving effect. Chin. J. Rock Mech. Eng., 31, S1, 3031–3037.

Wang, Y.: 2019, Experimental study on mechanical effect of limestone weakening under acid dissolution. Value Eng., 38, 7, 168–170.
DOI: 10.14018/j.cnki.cn13-1085/n.2019.07.050

Xu, M.F., Jiang, G.N., Jiang, T.F., Zhang, Z.L. and Yu, H.: 2020, A cumulative blasting damage model of rock based on Hoek-Brown criterion and its engineering application. Chin. J. Rock Mech. Eng., 39, S1, 2683–2692. DOI: 10.13722/j.cnki.jrme.2019.1062

Xu, M.F., Jiang, G.N., Zhang, Y. and Shen, F.Y.: 2021, A coupling damage model under Freeze-thaw cycles and loading based on Hoek-Brown criterion and its algorithm research. J. Basic Sci. Eng., 29, 3, 702–717. DOI: 10.16058/j.issn.1005-0930.2021.03.015

Zhang, Y.D., Xie, H.Q., Liu, H.Z., Xiao, M.S., Zhuo, L. and He, J.D.: 2021, Compound damage comnustitutive model and evolution characteristics of intermittent joint rock mass under high stress conditions based on Hoek-Brown criterion. Water Resources and Power, 39, 2, 109–113.
DOI: 10.20040/j.cnki.1000-7709.2021.02.027